JOURNAL OF THE ROYAL SOCIETY Interface

Insect-like flapping wing mechanism based on a double spherical Scotch yoke

Cezary GaliDski and RafaB {bikowski

J. R. Soc. Interface 2005 **2**, 223-235
doi: 10.1098/rsif.2005.0031

JOURNAL OF THE ROYAL SOCIETY Interface

J. R. Soc. Interface (2005) **2**, 223–235
doi:10.1098/rsif.2005.0031
Published online 18 May 2005

Insect-like flapping wing mechanism based on a double spherical Scotch yoke

Cezary Galiński[1] and Rafał Żbikowski[2,†]

[1]*Instytut Techniki Lotniczej i Mechaniki Stosowanej, Politechnika Warszawska, ul. Nowowiejska 24, 00-665 Warszawa, Poland*
[2]*Department of Aerospace, Power and Sensors, Cranfield University (RMCS Shrivenham), Swindon SN6 8LA, UK*

We describe the rationale, concept, design and implementation of a fixed-motion (non-adjustable) mechanism for insect-like flapping wing micro air vehicles in hover, inspired by two-winged flies (Diptera). This spatial (as opposed to planar) mechanism is based on the novel idea of a double spherical Scotch yoke. The mechanism was constructed for two main purposes: (i) as a test bed for aeromechanical research on hover in flapping flight, and (ii) as a precursor design for a future flapping wing micro air vehicle. Insects fly by oscillating (plunging) and rotating (pitching) their wings through large angles, while sweeping them forwards and backwards. During this motion the wing tip approximately traces a 'figure-of-eight' or a 'banana' and the wing changes the angle of attack (pitching) significantly. The kinematic and aerodynamic data from free-flying insects are sparse and uncertain, and it is not clear what aerodynamic consequences different wing motions have. Since acquiring the necessary kinematic and dynamic data from biological experiments remains a challenge, a synthetic, controlled study of insect-like flapping is not only of engineering value, but also of biological relevance. Micro air vehicles are defined as flying vehicles approximately 150 mm in size (hand-held), weighing 50–100 g, and are developed to reconnoitre in confined spaces (inside buildings, tunnels, etc.). For this application, insect-like flapping wings are an attractive solution and hence the need to realize the functionality of insect flight by engineering means. Since the semi-span of the insect wing is constant, the kinematics are spatial; in fact, an approximate figure-of-eight/banana is traced on a sphere. Hence a natural mechanism implementing such kinematics should be (i) spherical and (ii) generate mathematically convenient curves expressing the figure-of-eight/banana shape. The double spherical Scotch yoke design has property (i) by definition and achieves (ii) by tracing spherical Lissajous curves.

Keywords: insect-like flapping wings; micro air vehicles; flapping wing mechanism; spherical Lissajous curves; double spherical Scotch yoke

1. INTRODUCTION

This paper describes the rationale, concept, design and implementation of a spatial mechanism for micro air vehicles (MAVs) with insect-like flapping wings, inspired by two-winged flies (Diptera). The device focuses on the wing motion in hover and assumes a fixed motion envelope, i.e. the envelope cannot be adjusted once the device is assembled. The mechanism is based on the novel idea of a double spherical Scotch yoke, while the previous design, see Żbikowski *et al.* (in press), focused on a planar mechanism, utilizing a four-bar linkage. This work is part of a larger research effort at Cranfield University (RMCS Shrivenham) aimed at designing, building, testing and fielding a flapping wing micro air vehicle, see Żbikowski (1999*a*,*b*).

†Author for correspondence (r.w.zbikowski@cranfield.ac.uk).

The paper is organized as follows. This introduction continues by motivating the design in §1.1 and defining the design specifications in §1.2. The problem of defining insect-like wing tip kinematics in a realistic and practical way is then discussed in §2. Two idealized solutions are considered: Bernoulli's lemniscate in §2.1, and spherical Lissajous' curves in §2.2. It is concluded that the Lissajous approach is more attractive and can be realized mechanically by superposition of two sinusoidal motions, orthogonal to each other and with periods differing by a factor of two. A practical realization leads to a spatial mechanism based on a double spherical Scotch yoke, described in §3. The planar and spherical concepts are contrasted in §3.1, while the required drive train is presented in §3.2. The key elements of the design are described in §4, summarizing the stress analysis performed, presenting the moulds used for manufacturing and outlining the actual manufacturing of the yokes. Finally,

Received 16 December 2004
Accepted 10 February 2005

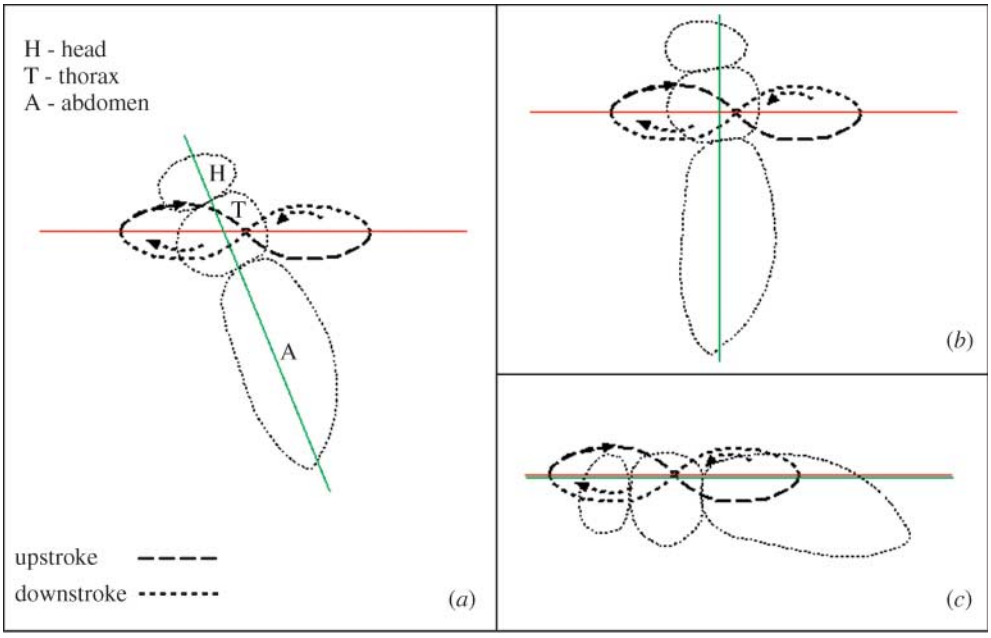

Figure 1. 'Generic' kinematics of insect in hover: the wing tip traces a 'figure-of eight', when seen from the insect side. The angle between the insect body axis (green) and the stroke plane (red) is constant. Typically, (*a*) the angle is steep; (*b*) one extreme: the angle is $\pi/2$ (see Żbikowski *et al.* in press); (*c*) the other extreme: the angle is zero (considered in this paper).

the functioning and testing of the complete mechanism is briefly highlighted in §5, and the conclusions follow in §6.

1.1. Motivation and background

MAVs are defined as flying vehicles approximately 150 mm in size (hand-held), weighing 50–100 g, and are being developed to reconnoitre in confined spaces (inside buildings, tunnels, etc.). This requires power-efficient, highly manoeuvrable, low-speed flight with stable hover. Such performance is routinely exhibited by flying insects and hence the focus on emulating insect-like flapping by engineering means. A detailed discussion of the future utility of MAVs and the advantages of considering insect-like flapping wing propulsion have been presented elsewhere, see Żbikowski (2000, 2002*a*). Here, we summarize the relevant basics of insect flight, emphasizing flapping wing kinematics and touching upon the complex aerodynamics involved.

Insects fly by oscillating (plunging) and rotating (pitching) their wings through large angles, while sweeping them forwards and backwards. The wingbeat cycle (typical frequency range: 5–200 Hz) can be divided into two phases: downstroke and upstroke (see figure 1*a*). At the beginning of downstroke, the wing (as seen from the front of the insect) is in the uppermost and rearmost position with the leading edge pointing forward. The wing is then pushed downwards (plunged) and forwards (swept) continuously and rotated (pitched) at the end of the downstroke, when the wing is twisted rapidly, so that the leading edge points backwards, and the upstroke begins. During the upstroke, the wing is pushed upwards and backwards and at the highest point the wing is twisted again, so that the leading edge points forward and the next downstroke begins.

Insect wing flapping occurs in a stroke plane that generally remains at the same orientation to the body, see figure 1*a*. The actual angle corresponding to the orientation is an interesting design parameter, so in Żbikowski *et al.* (in press) we considered the orthogonal arrangement, i.e. the angle of $\pi/2$, see figure 1*b*. In this work we focus on the parallel version, see figure 1*c*.

In hover—the focus of this work—the downstroke and upstroke are equal, resulting in the wing tip approximately tracing a figure-of-eight (as seen from the insect's side). However, the figure-of-eight is not necessarily generic, as other, less regular, closed curves with more than one or no self-intersections are also observed (e.g. Ennos 1989; Wakeling & Ellington 1997); for two-winged flies (Diptera) a 'banana' shape seems to be common. However, even for Diptera the kinematics in hover can be more complicated, so we settled on the figure-of-eight as 'commonly occurring' for reference purposes.

Since each half-cycle starts from rest and comes to a stop, the velocity distribution of the flapping is non-uniform, making the resulting airflow complex. It is also unsteady, i.e. the aerodynamic force varies in amplitude and direction during each wingbeat cycle. The variability of the force is compounded by the strong influence of the viscosity of air (owing to the small scale) and significant interaction of the wing with its wake (owing to hover). The details are explained elsewhere (Żbikowski 2002*b*); it is only noted here that the expected aerodynamic loading will be time-varying with magnitude peaks at the end of each half-cycle.

Finally, it is worth mentioning that the thorax–wing system in true flies (Diptera) is resonant (Pringle 1975), which contributes to the efficiency of propulsion. This feature was not implemented in the presented mechanism, but it is considered for a future design in the form of electro-mechanical resonance.

1.2. Design specifications

Not only are insect-like aerodynamics quite complex, but their observation and measurement in nature is very challenging (Willmott & Ellington 1997*a*,*b*; Willmott *et al.* 1997; Srygley & Thomas 2002). This motivated the development of aerodynamically scaled flapping mechanisms, most notably Ellington's flapper (van den Berg & Ellington 1997*a*,*b*) and Dickinson's Robofly (Dickinson *et al.* 1999). These devices allowed remarkable progress in gathering experimental data on insect-like aerodynamics (Ellington *et al.* 1996; Birch & Dickinson 2001). However, they tend to be bulky constructions not suitable for developing into light-weight, 150 mm versions suitable for a future flapping wing MAV.

On the other end of the scale, Fearing *et al.* (2000) and Avadhanula *et al.* (2002) aim at building an insect-like flapping robot weighing a tenth of a gram and with a 25 mm wing span. This approach is based on MEMS technology, as the expected forces (and payloads) are below 1 g.

In contrast to these efforts, the flapping mechanism described here was designed to the following specifications:

- miniature mechanism, no MEMS—the final vehicle is to be built on the 150 mm scale with 50–100 g weight, so the power required (a few watts) necessitates conventional mechanical engineering;
- fuselage 150 mm long and 25 mm in diameter—the mechanism must fit into a $150 \times 25\ \mathrm{mm}^2$ cylinder, the MAV dimensions compatible with the size of the human hand;
- design wingbeat frequency of 20 Hz—this is the lower threshold of audible sounds;
- fixed motion—the mechanism should implement predefined (as opposed to adjustable) kinematics of hover, so that the motion of each wing should be the mirror image of the other;
- biomimetic extraction—the mechanism should realize idealized insect-like flapping, implemented by engineering means;
- test bed for aerodynamic and mechanical aspects of flapping—the mechanism's main function is to foster research on aeromechanical aspects of insect-like flapping in hover, but it should also provide a precursor design for the final platform;
- durability versus weight—the need for a robust mechanism for prolonged testing takes precedence over weight optimization;
- spatial mechanism realization—use a spherical mechanism naturally to implement the required kinematics;
- stroke plane parallel to the fuselage—the wings should flap in a plane containing the long axis of the fuselage for ease of testing and handling, see figure 1;
- rotary DC motor propulsion—for ease of use and power efficiency;
- low cost—where possible, the use of off-the-shelf parts should be considered, drawing upon clock- and watch-making and hobby industries.

2. IDEALIZED WING TIP KINEMATICS

As outlined in §1.1, insect wing kinematics are essentially spherical, while the trace of the wing tip is usually photographed from the insect's side. The result is an orthogonal projection of the spherical trace on to the plane of the animal's longitudinal symmetry. The resulting planar figure for a hovering insect's wing is always closed. As far as can be discerned from the available (noisy) data, e.g. for flies (Ennos 1989), the actual shape may be a figure-of-eight or a banana shape, but can be irregular and sometimes the trace has no self-intersections. Owing to the inherent experimental difficulties, the kinematic and aerodynamic data from free-flying insects are sparse and uncertain, and it is not clear what aerodynamic consequences different wing motions have, despite notable progress (e.g. Dickinson *et al.* 1998; Lehmann & Dickinson 1998; Lehmann 2004). Since acquiring the necessary kinematic and dynamic data remains a challenge, a synthetic, controlled study of insect-like flapping is not only of engineering value, but also of biological relevance.

There are two phases in each half-cycle of the wing beat: translational (wing moving forwards or backwards) and rotational (at the end of each stroke). In order to clearly investigate the distinct aerodynamic contributions of each phase, the angle of attack should be constant during translation and rotate through at least 90° during the flip-over. Thus, theoretically attractive kinematics should entail an intermittent rotational motion with reversal. A more subtle aspect is the plunging (up–down) component of flapping. Every time a hovering wing starts (or stops) it sheds a starting (stopping) vortex (Wagner 1925; Żbikowski 2002*b*) which is then convected according to the airflow evolution. Despite the convection, such a vortex may persist in the vicinity of its original shedding point when the wing revisits that point in the next half-cycle. Then the wing and the vortex will collide and the flow structure is impaired. However, if the wing plunges up and down while moving forwards and backwards, it may be able to avoid hitting the vortex when revisiting the shedding point. In other words, figure-of-eight kinematics—with the width of the 'eight' corresponding to the extent of plunging—can plausibly be advantageous[1] for aerodynamic reasons. Hence the focus of this work has been idealized wing tip kinematics of that type, so that the results are practical to implement, but scientifically relevant both for engineers and biologists.

For ease of analysis, it has been decided to implement wing tip kinematics as a spherical, symmetric, self-intersecting curve, which would admit a convenient mathematical description and a simple engineering realization. Two options were considered: (i) Bernoulli's lemniscate and (ii) spherical Lissajous curves.

[1]The authors are grateful to Mr Salman Ansari for pointing out this possible advantage of figure-of-eight kinematics.

2.1. Bernoulli's lemniscate

Lemniscates are level curves of polynomials (Brieskorn & Knörrer 1986). They are plane algebraic curves of order $2n$, such that the product of the distances of each point of the curve from n given focuses $F_1, \ldots, F_n$, is equal to the nth power of the radius r. In the complex plane notation this means

$$|(z - z_1)\ldots(z - z_n)| = r^n, \quad z = x + \mathrm{i}y, \quad r > 0, \tag{2.1}$$

where z_i are the coordinates of the focuses F_i. A figure-of-eight type curve will have $n=2$ focuses and the example considered was Bernoulli's lemniscate:

$$0 = (x^2 + y^2)^2 - a^2(x^2 - y^2), \tag{2.2}$$

$$(x(t), y(t)) = \left(\frac{a\cos t}{1+\sin^2 t}, \frac{a\sin t\cos t}{1+\sin^2 t}\right), \quad t \in [0,2\pi], \tag{2.3}$$

with the focuses at $(-d, 0)$ and $(d, 0)$, where $a = d\sqrt{2}$. The focus on Bernoulli's lemniscate was due to: (i) its connection with Viviani's curve (a spherical figure-of-eight), and (ii) its ready realization with a four-bar linkage (see Hartenberg & Denavit 1964, p. 79; Dijksman 1976, ch. 11).

Since the insect wing has constant span and is hinged at the root, its tip traces a figure-of-eight on a sphere, and the photographs register the orthogonal projection of this spherical curve on to a plane. Bernoulli's lemniscate naturally generalizes to the sphere in the simple form of Viviani's curve (see figure 2):

$$\left.\begin{aligned} x(t) &= a\cos^2 t, \\ y(t) &= a\cos t\sin t, \\ z(t) &= a\sin t, \quad t \in [0,2\pi], \end{aligned}\right\} \tag{2.4}$$

which is the intersection of the sphere $x^2+y^2+z^2=a^2$ and the cylinder $x^2+y^2=ax$. The lemniscate of equation (2.3) generates equation (2.4) via a stereographic projection[2] from the antipode of the double (self-intersection) point of Viviani's curve. Furthermore, the orthogonal projection of Viviani's curve on the yz-plane is Gerono's lemniscate (Lawrence 1972, pp. 124–126):

$$\left.\begin{aligned} y(t) &= a\cos t\sin t \\ z(t) &= a\sin t, \quad t \in [0,2\pi], \end{aligned}\right\} \tag{2.5}$$

as is readily seen by putting $x=0$ in equation (2.4), and corresponds to $z^4 - a^2(z^2 - y^2) = 0$.

Thus, in principle, if a planar mechanism generates Bernoulli's lemniscate, then (via a spherical joint) the wing tip will trace Viviani's curve, and its flat trace will be Gerono's lemniscate. Since all of these curves are described by simple, closed-form formulae (2.3)–(2.5), the kinematic analysis becomes trivial.

The crank-rocker, non-Grashof, four-bar linkage with proportions $1:\sqrt{2}:1$ has Bernoulli's lemniscate as its coupler curve (Hartenberg & Denavit 1964, p. 79; Dijksman 1976, ch. 11). In this set-up, the centre point of the coupler makes excursions beyond the base endpoints. Thus, to avoid tripping on one another, the links must be stacked up in layers, an inefficient use of space. Even with the layered arrangement, a protrusion from *both* sides of the centre point, orthogonal to the linkage plane, would block the mechanism's movement. Such protrusion is needed to drive both wings from a single mechanism. The alternative of two mechanisms (one for each wing), each made of links stacked up in layers, is impractical owing to excessive complexity and prohibitive use of space. Hence, despite its mathematical ease and elegance, the approach was judged not feasible from the engineering viewpoint. Also, this concept is unable to produce banana-shaped curves.

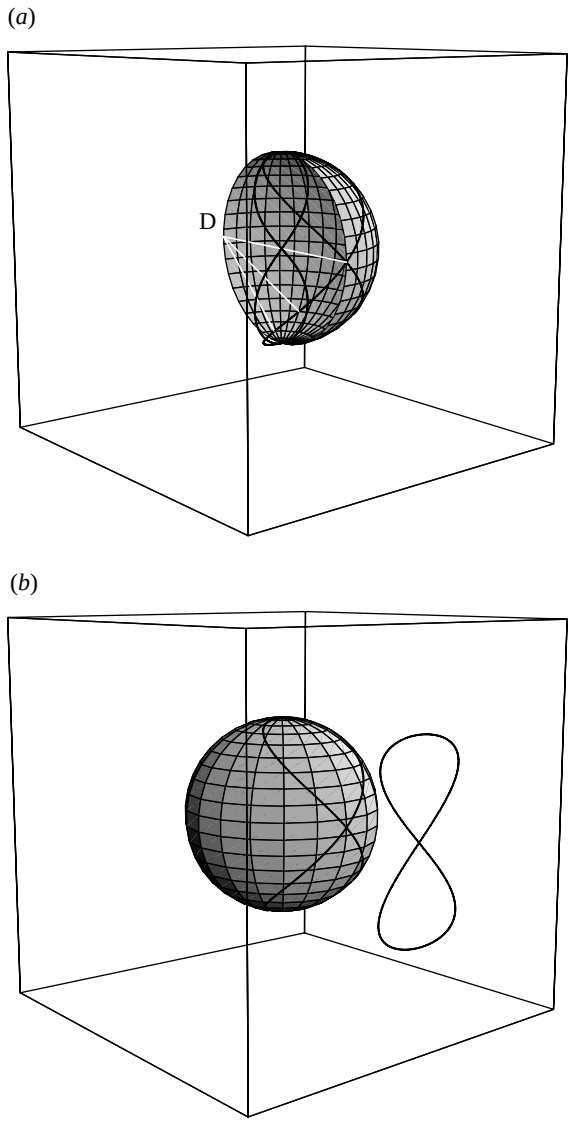

Figure 2. Bernoulli's lemniscate based figure-of eight curves: (*a*) Viviani's curve can be obtained by the stereographic projection of the planar lemniscate of Bernoulli from the point D; this point is the antipode of the double point of Viviani's curve; (*b*) the orthogonal projection of Viviani's curve onto the yz-plane is a planar figure-of eight, known as Gerono's lemniscate.

[2]Referring to figure 2, this means that the ray emanating from D follows Bernoulli's lemniscate and traces Viviani's curve on the sphere.

The implementation difficulties arising from implementation of Bernoulli's lemniscate can be alleviated if the classical straight-line mechanism of Watt (e.g. Hartenberg & Denavit 1964, p. 79; Dijksman 1976, ch. 3) is considered, as we have described in Żbikowski *et al.* (in press). This double-rocker four-bar linkage produces families of curves of the figure-of-eight type according to the link proportions chosen. Also, a horizontally oriented linkage generates the coupler curve orthogonally to its base, so it can be housed in a cylindrical fuselage. Furthermore, the links will not make excursions beyond the housing owing to the double-rocker configuration.

While figure-of-eight lemniscates are quadrics, the straight-line mechanism curves are sextics and do not admit particularly convenient parametrizations (Hartenberg & Denavit 1964; Rutter 2000). Still, a closed form expression is available (Wunderlich 1978) and a formula for the corresponding spherical curve can be derived. However, it is not possible to generate banana-shaped curves with the straight-line mechanism.

2.2. Lissajous curves

Since the theoretically attractive approach of §2.1 turned out to be impractical, an alternative was sought that would provide mathematical simplicity and mechanical realizability. A straightforward solution was to consider the well-known Lissajous curves. They arise by the composition of two sinusoidal waveforms in orthogonal directions, i.e. by composing $\sin \omega t$ perpendicularly with $a \sin(k\omega t + \alpha)$.

There is no standard way of generalizing planar Lissajous curves to spatial ones. One way, useful in knot theory (Bogle *et al.* 1994), is to consider

$$\left.\begin{aligned} x(t) &= \sin(\omega_x t + \alpha_x), \\ y(t) &= \sin(\omega_y t + \alpha_y), \\ z(t) &= \sin(\omega_z t + \alpha_z), \end{aligned}\right\} \tag{2.6}$$

which results in a wealth of three-dimensional curves. However, a more natural approach, in keeping with the spherical nature of the required motion, is simply to specify orthogonal sine waves directly in the spherical coordinates:

$$\left.\begin{aligned} r(t) &= R, \\ \theta(t) &= \theta_{\max} \sin \omega t, \\ \phi(t) &= a\theta_{\max} \sin(k\omega t + \alpha) + \phi_{\text{offset}}, \end{aligned}\right\} \tag{2.7}$$

where $R = \text{const.}$ is the radius of the sphere and $\theta_{\max} \in (0, \pi/2)$ in order for the curve to be confined to a hemisphere, while ϕ_{offset} should take values 0, $\pi/2$, or π to choose the desired hemisphere. The θ-sinusoid is the reference and thus the ϕ-sinusoid is defined with respect to it by the constants $a \in (0,1]$, $k = 1, 2, \ldots$, and $\alpha \in [0, \pi/2]$.

Since equation (2.7) is related to the Cartesian coordinates in the usual way,

$$\left.\begin{aligned} x(t) &= r(t) \cos\theta(t) \sin\phi(t), \\ y(t) &= r(t) \sin\theta(t) \sin\phi(t), \\ z(t) &= r(t) \cos\phi(t), \end{aligned}\right\} \tag{2.8}$$

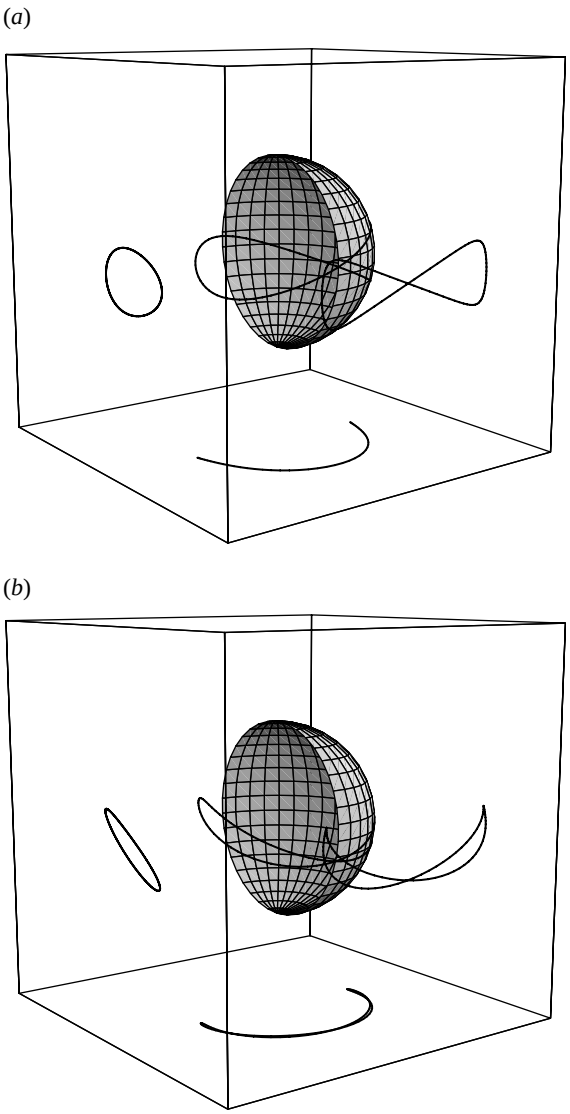

Figure 3. Spherical Lissajous curves with a single intersection (double point). (*a*) A spherical figure-of-eight and its orthogonal projections; note the 'hour-glass' shape of the projection on to the plane of the longitudinal symmetry. (*b*) A spherical banana trace and its orthogonal projections; the cusps of the side projection are two-dimensional artefacts: the spherical curve is smooth.

two-dimensional projections of the spherical Lissajous curves are readily obtained. This is illustrated in figure 3. It is worth noting that not only can a spherical figure-of-eight be generated (figure 3*a*), but also a spherical banana shape is possible (figure 3*b*).

Finally, mechanical realization of the composition of two sinusoidal waveforms in orthogonal directions is possible by a generalization of the classical Scotch yoke, as described in §3 below.

3. SCOTCH YOKE MECHANISM FOR LISSAJOUS SPHERICAL FIGURE-OF-EIGHT

As described in Żbikowski *et al.* (in press), we have successfully used a planar four-bar linkage with a spatial articulation to implement an insect-like flapping mechanism. Therefore, a spherical four-bar linkage seemed a natural way of progressing to a spatial design.

According to Chiang (1992), many features of planar four-bar linkages can be observed in the case of their spherical counterparts, or at least have appropriate analogies. In particular, spherical linkages are capable of generating symmetrical coupler curves (see Lu & Hwang 1996). A symmetrical, spherical double rocker linkage should be similar to the corresponding planar version used in Żbikowski *et al.* (in press). However, that planar mechanism was transitional (Hunt 1978, ch. 7), i.e. it had kinematic singularities. This means that it had an uncertainty configuration when transitioning between a Grashof and a non-Grashof kinematic chain. In other words, when the coupler is momentarily collinear with another link, it can either continue its previous motion or suddenly reverse the direction. This mathematical singularity can lead to surprisingly diverse coupler curves (Torfason & Ahmed 1978; Hernandez *et al.* 1994; Pennestri 1998).

In the case of planar four-bar linkage we overcame this problem by the application of springs forcing the driven rocker to the central position and appropriately selected tolerances, see Żbikowski *et al.* (in press). However, linkage had to be led between two vertical planes to avoid uncontrolled motions in the direction orthogonal to the linkage plane. This arrangement, or its equivalent, would not be easy to achieve in spherical geometry, as two concentric spheres should be used to obtain a similar effect. Hence we concluded that, as a solution, a spherical double rocker linkage would be too complicated and too expensive. However, a certain combination of spherical four-bar linkages appeared to be feasible as a spherical flapping mechanism. Two conic Scotch yokes and a universal joint can be used to generate desired kinematics. Each can be interpreted as a particular case of the spherical four-bar linkage, see Crossley (1955).

3.1. Planar versus spherical double Scotch yoke

A spherical figure-of-eight together with decoupled pitching is easily obtainable if each of them have a common apex and if both Scotch yokes are orthogonal. This combination allows the creation of Lissajous' curves if yokes are driven by sinusoidal inputs, one twice as fast as the other. As a result, a smooth figure-of-eight motion can be obtained, without any excessive accelerations, thus decreasing dynamic loads. The first step was to propose a planar mechanism capable of converting rotary input into reciprocal motion of the figure-of-eight type. This was done by combining orthogonally two Scotch yokes, so that Lissajous curves were generated.

One of the yokes moves up and down, while the other moves back and forth, see figure 4*a*. This way, two orthogonal sine waves are produced, and if their frequency ratio is 2:1, Lissajous curves will be produced. The actual shapes of the resulting figure-of-eight curves depend not only on sine amplitudes, but also on phase differences.

The planar double Scotch yoke can be sensitive to manufacturing quality and can be locked, if linear bearings are not sufficiently parallel, or owing to asymmetric loads, if the frame is not sufficiently rigid.

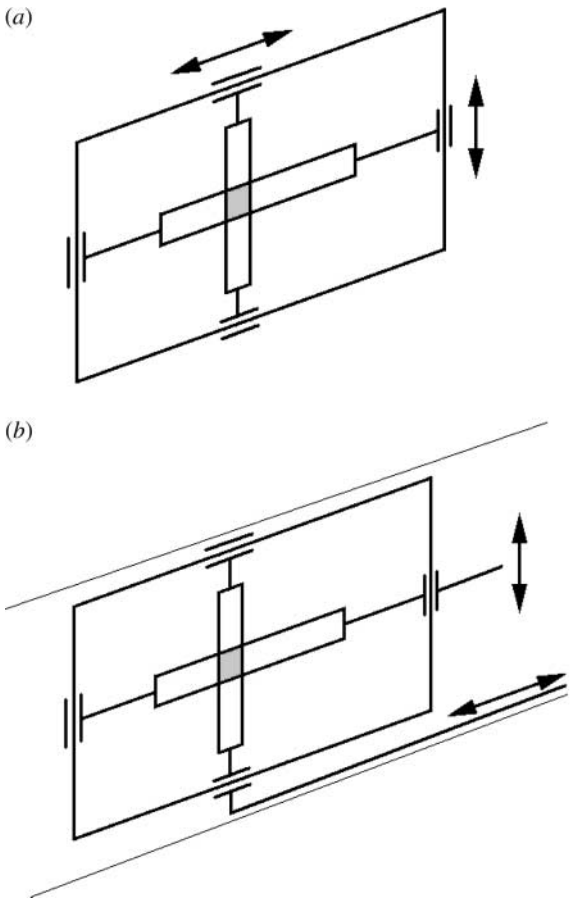

Figure 4. Planar double Scotch yoke: (*a*) kinematic diagram; (*b*) realistic driving method in constrained volume.

It is not straightforward to drive the double Scotch yoke in a constrained volume if symmetric forces are to be used. In particular, the horizontal yoke has to be driven from one side only if the mechanism has to fit into the tube with the small diameter as required in the case of MAV, see figure 4*b*.

The drawbacks of the planar double Scotch yoke, described in §3.1, can be avoided if the yokes are made spherical and their translation is exchanged with their rotation. In this configuration, both ends of each yoke are rotated about the same axis, see figure 5*a*. The figure-of-eight generated is then spherical by default, significantly simplifying wing articulation, see figure 5*b*.

In figure 6, note that axle E1 is attached to frame component A5a by two plates A5b, so that a mode of slide bearing is created. The axle is equipped with two universal joints for wing articulation and a lever for pitch control. Wings can be attached to the tubes at both axle ends. Yokes C1 and B1 are also attached to frame component A5a, so that their axes cross in the centre of the universal joint. The mechanism contains two universal joints and two sets of yokes, to which two wings are to be attached. Universal joints cannot have a common centre, since the lever and attachment bearings have to be located between them.

This is the heart of the proposed flapping mechanism.

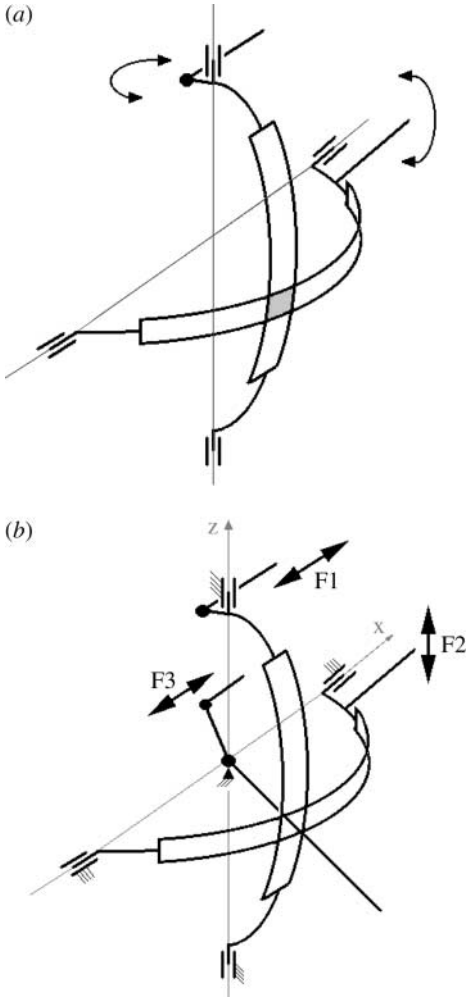

Figure 5. Spherical double Scotch yoke: (*a*) kinematic diagram; (*b*) concept of the associated flapping mechanism, see also figure 6.

3.2. Drive train

The spherical double Scotch yoke needs to be driven either by moments acting about its axes, or by a pair of forces acting between axes and pins attached to yokes, see figure 5*a*. Both yokes are equipped with suitable pins and are driven by linear sliders, see figure 7. Vertical yoke C1 is driven by horizontal slider C2, while horizontal yoke B1 is driven by vertical slider B2. Both sliders have slots suited to drive yokes. The pitch controlling lever is driven by pusher E2.

As illustrated in figure 8, horizontal slider C2 is connected to frame component A3 by a linear bearing C4. Vertical slider B2 is placed between frame components A5a, A1 and A2. Slider C2 is driven by crank C3b which is part of assembly C3. Slider B2 is driven by crank B3b which is part of assembly B3. Assemblies C3 and B3 also contain helical gears. These gears are connected by a helical gear from assembly D2. Axes of all these gears are orthogonal. Pitch diameters have the proportions 1:1:2 (B3:D2:C3). Assembly B3 is driven by a DC motor through connector D1, so that assemblies B3 and D2 rotate with the same velocity, while assembly C3 rotates twice as slowly. One rotation of C3 assembly generates a complete figure-of-eight.

Assembly D2 drives the Geneva wheel pitch reversal generator. The Geneva wheel driver has one arm, so that the Geneva wheel switches the pitch twice during the mechanism cycle.

Exploded views of the complete mechanism are presented in figure 8, and a photograph of the assembled mechanism is given in figure 9.

4. MECHANISM ENGINEERING

The most challenging aspect of the mechanism design was the spherical yokes.

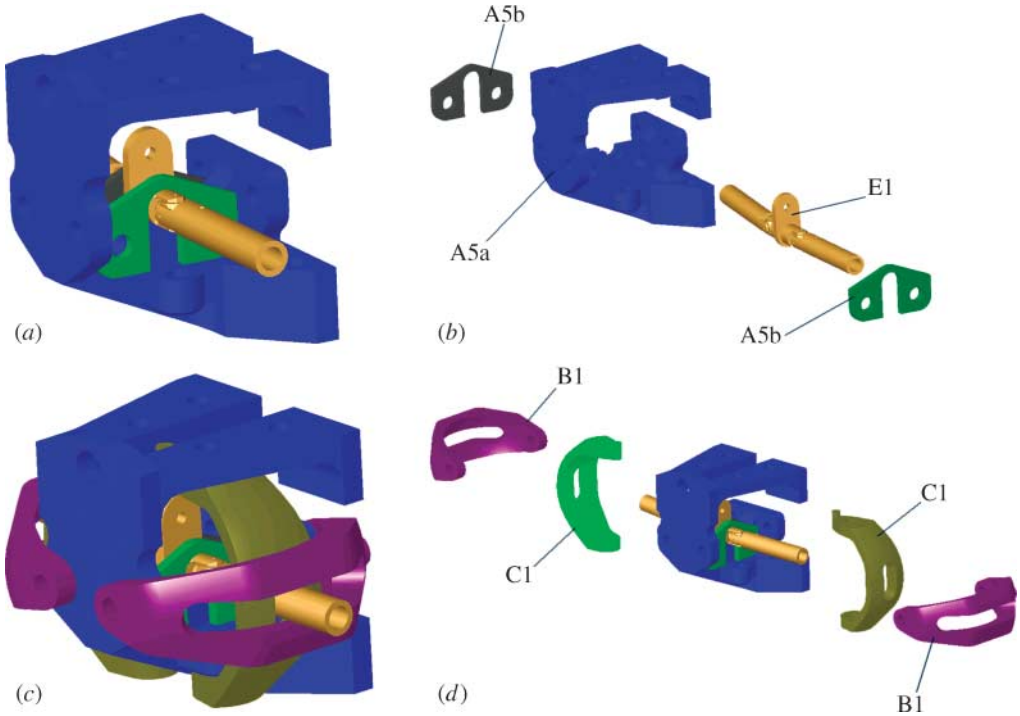

Figure 6. Practical realization of spherical double Scotch yoke; for description, see text.

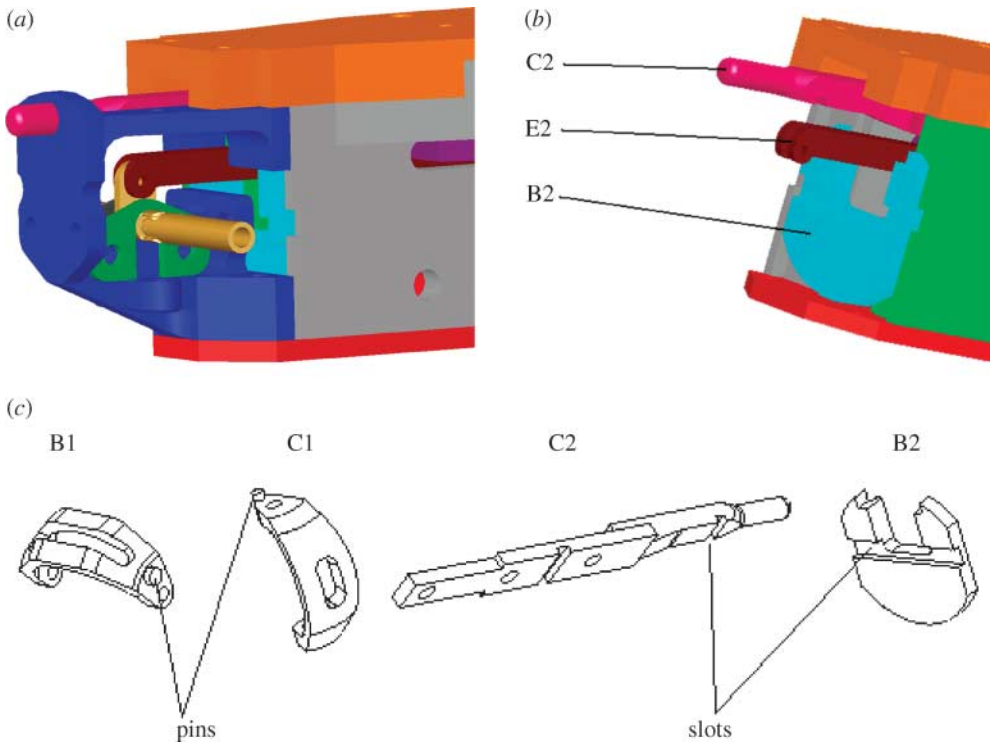

Figure 7. Details of the driving components; for description, see text.

In contrast with our four-bar mechanism (Żbikowski *et al.* in press), the current design generates Lissajous' curves and does not experience excessive accelerations. The flapping is much smoother, so inertial loads are relatively small and the aerodynamic loads dominate in this case. The details of the aerodynamic loads are given elsewhere (Żbikowski 2002*b*; Żbikowski *et al.* in press), so here we present only the results of strength analysis.

As expected, the yokes were the most heavily loaded parts. That was owing to small distances between axes and driving pins and the presence of large slots. Moreover, the yokes carry most of the load especially for the highest considered flapping frequency of 20 Hz and largest considered (150 mm) wing, see figure 10. Since the maximum stress is of the order of 1200 MPa near the driving pins, the best quality steel with heat treatment would be required (see stress values in figure 10). However, the yokes are quite small and have curved, three-dimensional shape. In particular, the horizontal yoke could be difficult to machine in such small scale owing to the spherical character of the internal surface. Heat treatment would make machining problems even worse and would lead to deformation and possible cracks. Therefore, it was decided to make yokes out of carbon–epoxy composite.

4.1. Yokes design and manufacturing

Small dimensions created manufacturing problems in this case as well, but they were not prohibitive. The simplest and most precise method to make the moulds would be via rapid prototyping. Since it was not readily available, ordering the moulds from an external contractor was expected to be too expensive and time-consuming. Therefore, it was decided to make moulds for the first prototype with application of a more classical method: the ball from a ball bearing was used as a model of the spherical surface, see figure 11*a*,*b*. However rapid prototyping is considered for future designs.

Tex 1610 strands of Tenax HTA carbon fibres were used to make the yokes, together with L epoxy resin and L hardener from R&G for impregnation. Carbon is known as a perfect material for friction brake blocks, but wearing characteristics of available carbon/epoxy compositions were not known. Moreover, one axle surface required low friction, since it was designed as a plain bearing, while the other required threading. That is why it was decided to include brass sleeves into the yoke structure, see figure 11*c*. One of these had an internal diameter of 2 mm and wall thickness of 0.1 mm, a second had internal diameter of 1.6 mm and a wall thickness 0.3 mm. Both sleeves were installed on the axle rod at the beginning of the manufacturing process. The strand of fibres was impregnated out of the mould and then laid down inside. It surrounded the sleeves and the 'tongue' simulating slot, see figure 12. The strand was crossed several times in the course of the process, providing maximum possible strength and filling the mould to the maximum possible extent. However, small volumes were not filled on both ends of the 'tongue' and in the area close to the sleeves. These volumes had to be filled with aerosil/epoxy composition.

After curing, the mould was opened and the yoke was taken out. Excess material was cut and a thicker sleeve threaded. The yoke was then ready for assembly.

The technology described above is workable, but not simple, and it requires significant experience. Also, the air bubbles left in the structure (see figure 11*c*) prove that it is not perfect yet. Therefore, other technologies will be considered for the future, particularly in the case of serial manufacturing. Injecting the filaments mixed

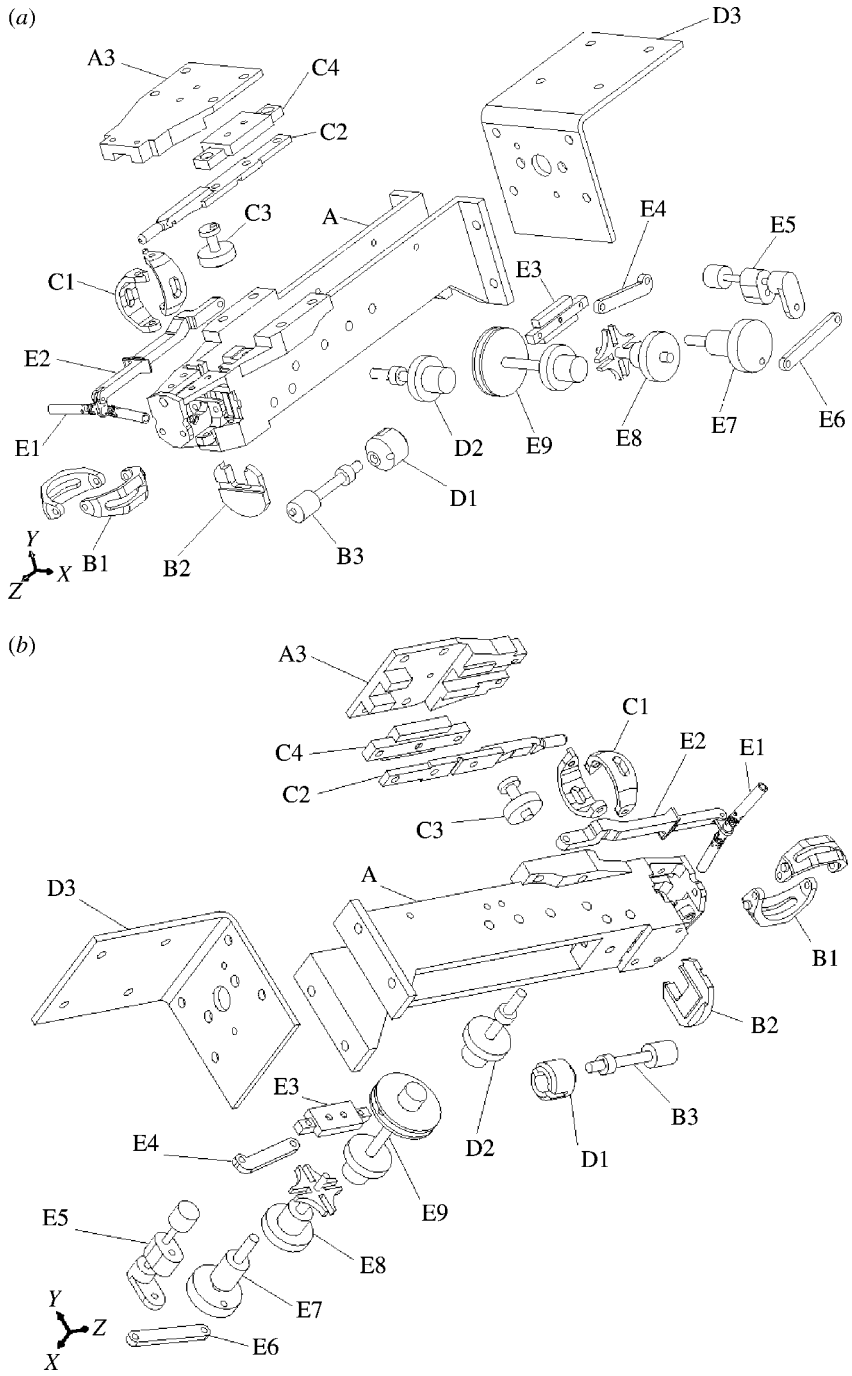

Figure 8. Exploded views of the complete mechanism.

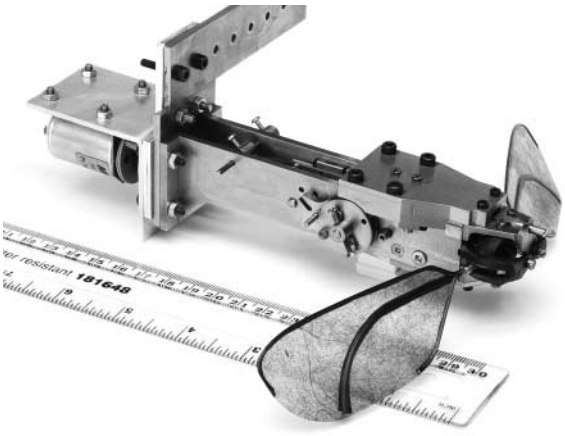

Figure 9. General view of the complete mechanism.

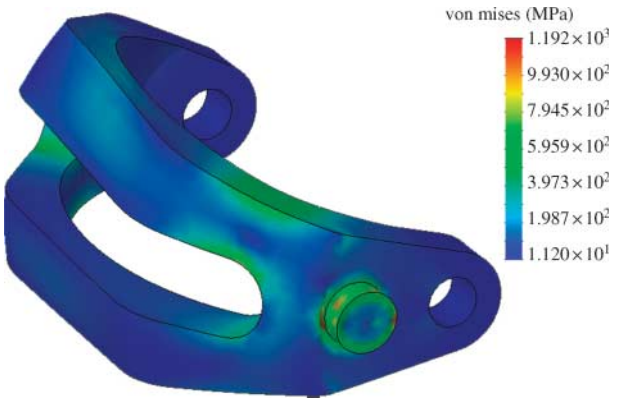

Figure 10. Maximum stress in the horizontal yoke for the flapping frequency of 20 Hz and a 150 mm wing.

Figure 11. (*a*) Bearing ball used as a prototype of the yokes' spherical surface together with the negative of the half-sphere made in first phase of prototyping. (*b*) Vertical yoke mould components; note the metallic rod used to model the axle surfaces. (*c*) The vertical yoke ready for assembly.

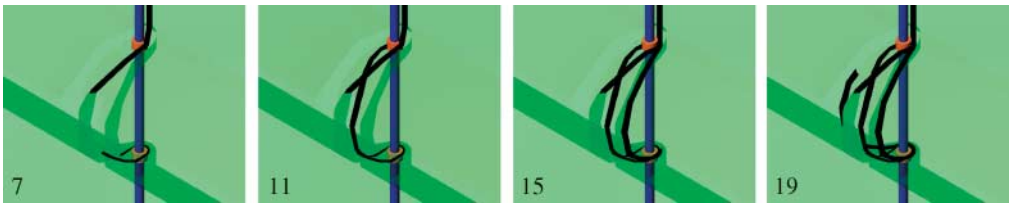

Figure 12. Sequence (selected frames) of laying down the carbon strand in the mould.

with the matrix would be the best possible technology for yoke manufacturing. However, a composition providing sufficient strength has yet to be developed. Perhaps nanotubes composite would be optimal for this application, but a proper matrix would have to be chosen first. Also, the yokes' wearing has to be studied, particularly around the pins. Experiments conducted so far have shown that some metallic components of the mechanism wear out faster than the yokes' pins.

5. MECHANISM FUNCTIONING AND TESTING

Figure 9 shows the mechanism assembled and ready for testing. As a first step, functionality testing was performed proving that the mechanism generally works as required.

The only problem discovered so far was that axle E1 was built of two off-the-shelf universal joints and the brass lever. All these three components were glued together. Gluing appeared not to be as robust as desired. Therefore, the axle will be redesigned or its bonding technology changed in the future. Candidate technologies considered are soldering or electron beam welding.

Despite this weakness, it was possible to perform preliminary particle image velocimetry (PIV) flow measurements. A stereoscopic PIV system was used in which two imaging cameras photographed a common

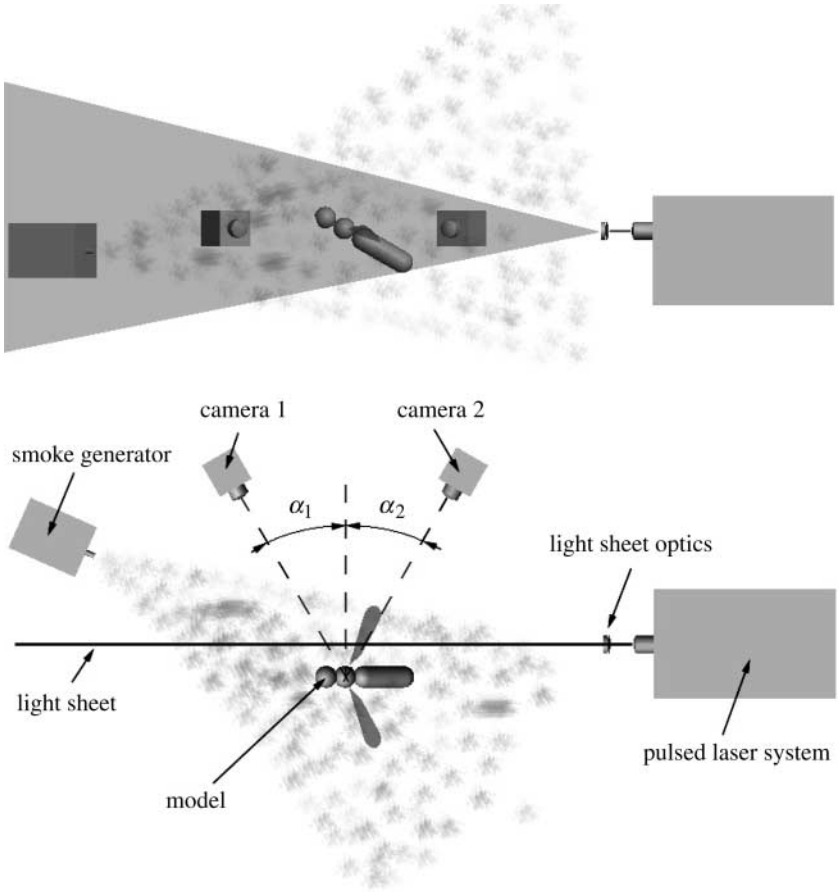

Figure 13. Stereoscopic PIV system used for flow visualization and to verify the figure-of-eight kinematics, see figure 14.

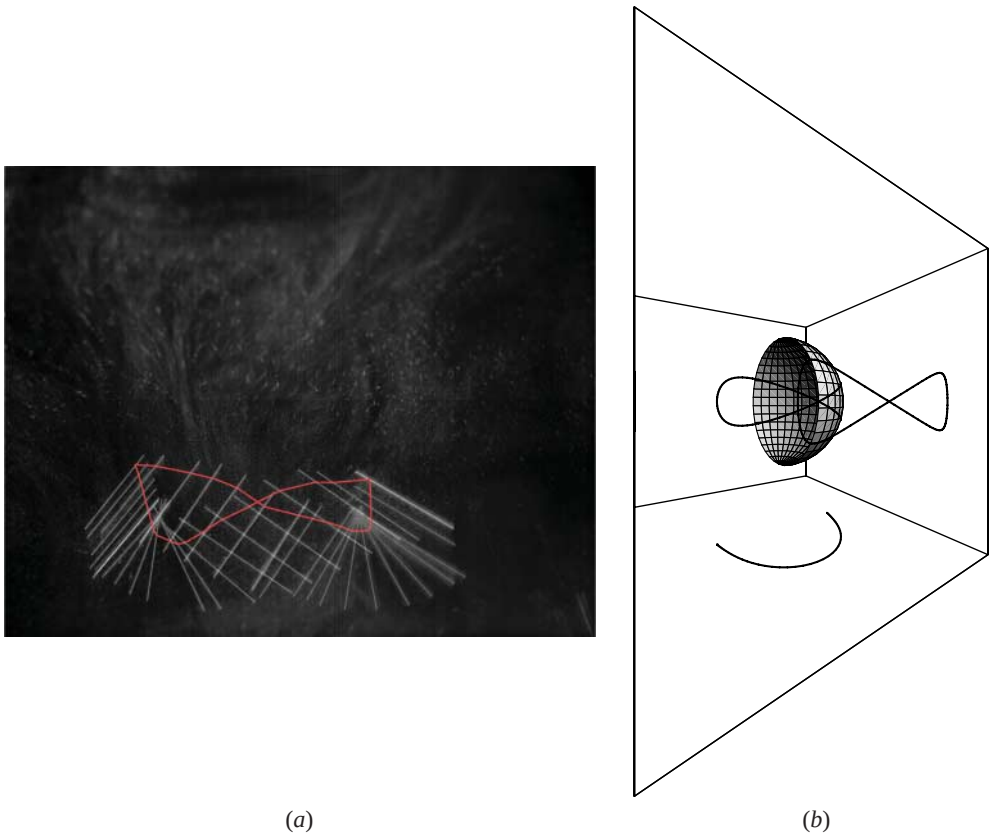

(*a*) (*b*)

Figure 14. Comparison of (*a*) the mechanically realized figure-of-eight with (*b*) the theoretical plot of the designed shape, seen from approximately the same perspective, see also figure 3.

measurement area illuminated by a pulsed laser. This set-up allowed inference of the third (out of plane) velocity component from observation of the plane defined by the sheet of laser light, see figure 13.

As a by-product of the collected aerodynamic data it was possible to verify the figure-of-eight shape produced by the mechanism, see figure 14. Figure 14*a* was created by combining several subsequent frames from a single camera. It shows the path created by the intersection point of the light sheet and wing axis of rotation; subsequent wing sections are also visible. Figure 14*b* is a theoretical plot of the designed path seen from approximately the same perspective as in figure 14*a*. This comparison of the assumed spherical Lissajous curve and its mechanical realization demonstrates correctness of the design.

PIV experiments were performed in a cumulative time of approximately 1 h, without any failures. This result is quite satisfactory, since experiments provided useful aerodynamic data and 1 h is approximately the required time of robust functioning of the mechanism.

6. CONCLUSIONS

The kinematics of an insect-like flapping wing for MAVs requires three-dimensional motion which is essentially spherical in character. Spherical double Scotch yoke is a relatively simple mechanism, complying with this requirement and realizing the required figure-of-eight as a spherical Lissajous' curve.

The spherical double Scotch yoke mechanism on the MAV scale was designed, manufactured, assembled and tested. It was found to be quite reliable and met its specifications, performing satisfactorily in tests and generating useful data for further aeromechanical studies. The few problems discovered in the course of the testing are minor and can be resolved by viable modifications.

Initial aerodynamic data have been gathered and more tests, both for force measurement and flow visualization, are planned. The new data will allow a quantifiable study of the aeromechanics of insect-like flapping at the MAV scale. It will also generate information of value for the analysis of insect flight, where similar experiments are difficult to perform. Finally, the progress in understanding of the aeromechanics of insect-like flapping wings will be used to gain additional insights into the flight of real insects. Thus, an engineering study inspired by nature will contribute to a better understanding of nature which, in turn, can be used to further progress the engineering design. This fruitful cycle seems to be a good and practical example of the real value of the interface between engineering and biology.

This work was supported by the U.S. Army (European Research Office) under Contract N62558-03-M-0030. We thank Dr Nick Lawson for his assistance with PIV experiments in which a pair of high-speed cameras were used. The cameras were sponsored by DARPA (Sam Wilson from the Tactical Technology Office) and loaned to us by NASA Langley Research Center (Dynamics and Control Branch; special thanks to Marty Waszak).

We thank the referees for their helpful comments and attention to detail, which improved the quality and clarity of the final version.

REFERENCES

Avadhanula, S., Wood, R., Campolo, D. & Fearing, R. 2002 Dynamically tuned design of the MFI thorax. In *Proc. IEEE International Conference on Robotics and Automation, ICRA'02*, vol. 1, pp. 52–59. Piscataway, NJ: IEEE.

Birch, J. M. & Dickinson, M. H. 2001 Spanwise flow and the attachment of the leading-edge vortex on insect wings. *Nature* **412**, 729–733.

Bogle, M. G. V., Hearst, J. E., Jones, V. F. R. & Stoilov, L. 1994 Lissajous knots. *J. Knot Theor. Ramif.* **3**, 121–140.

Brieskorn, E. & Knörrer, H. 1986 *Plane algebraic curves*. Basel: Birkhäuser.

Chiang, C. H. 1992 Spherical kinematics in contrast to planar kinematics. *Mech. Mach. Theory* **27**, 243–250.

Crossley, F. R. E. 1955 3-D mechanisms. *Mach. Des.* **27**, 175–179.

Dickinson, M. H., Lehmann, F. O. & Chan, W. P. 1998 The control of mechanical power in insect flight. *Am. Zool.* **38**, 718–728.

Dickinson, M. H., Lehmann, F. O. & Sane, S. P. 1999 Wing rotation and the aerodynamic basis of insect flight. *Science* **284**, 1954–1960.

Dijksman, E. A. 1976 *Motion geometry of mechanisms*. Cambridge: Cambridge University Press.

Ellington, C. P., van den Berg, C., Willmott, A. P. & Thomas, A. L. R. 1996 Leading-edge vortices in insect flight. *Nature* **384**, 626–630.

Ennos, A. R. 1989 The kinematics and aerodynamics of the free flight of some Diptera. *J. Exp. Biol.* **142**, 49–85.

Fearing, R. S., Chiang, K., Dickinson, M., Pick, D., Sitti, M. & Yan, J. 2000 Wing transmission for a micromechanical flying insect. In *Proc. IEEE International Conference on Robotics and Automation, ICRA'00*, vol. 2, pp. 1509–1516. Piscataway, NJ: IEEE.

Hartenberg, R. S. & Denavit, J. 1964 *Kinematic synthesis of linkages*. NewYork: McGraw-Hill.

Hernandez, A., Amezua, E., Ajuria, M. B. & Llorente, J. I. 1994 Multiple points on the coupler curve of transitional four-hinge planar linkages. *Mech. Mach. Theory* **29**, 1015–1032.

Hunt, K. H. 1978 *Kinematic geometry of mechanisms*. Oxford: Clarendon Press.

Lawrence, J. D. 1972 *A catalog of special plane curves*. New York: Dover Publications.

Lehmann, F. O. 2004 Aerial locomotion in flies and robots: kinematic control and aerodynamics of oscillating wings. *Arthropod Struct. Dev.* **33**, 331–345.

Lehmann, F. O. & Dickinson, M. H. 1998 The control of wing kinematics and flight forces in fruit flies (*Drosophila* spp.). *J. Exp. Biol.* **201**, 385–401.

Lu, D.-M. & Hwang, W.-M. 1996 Spherical four-bar linkages with symmetrical coupler-curves. *Mech. Mach. Theory* **31**, 1–10.

Pennestri, E. 1998 The transition curve of the planar four-bar: an analytical approach. *Mech. Mach. Theory* **33**, 1293–1299.

Pringle, J. W. S. 1975 *Insect flight*. Oxford Biology Readers, vol. 52. Glasgow: Oxford University Press.

Rutter, J. W. 2000 *Geometry of curves*. Boca Raton: Chapman & Hall/CRC.

Srygley, R. B. & Thomas, A. L. R. 2002 Unconventional lift-generating mechanisms in free-flying butterflies. *Nature* **420**, 660–664.

Torfason, L. E. & Ahmed, A. 1978 Double points of a 4-bar linkage. *Mech. Mach. Theory* **13**, 593–601.

van den Berg, C. & Ellington, C. P. 1997*a* The three-dimensional leading-edge vortex of a 'hovering' model hawkmoth. *Phil. Trans. R. Soc. B* **352**, 329–340.

van den Berg, C. & Ellington, C. P. 1997*b* The vortex wake of a 'hovering' model hawkmoth. *Phil. Trans. R. Soc. B* **352**, 317–328.

Wagner, H. 1925 Über die Entstehung des dynamischen Auftriebes von Tragflügeln. *Z. Angew. Math. Mech.* **5**, 17–35.

Wakeling, J. M. & Ellington, C. P. 1997 Dragonfly flight. II. Velocities, accelerations and kinematics of flapping flight. *J. Exp. Biol.* **200**, 557–582.

Willmott, A. P. & Ellington, C. P. 1997*a* Measuring the angle of attack of beating insect wings: robust three-dimensional reconstruction from two-dimensional images. *J. Exp. Biol.* **200**, 2693–2704.

Willmott, A. P. & Ellington, C. P. 1997*b* The mechanics of flight in the hawkmoth *Manduca sexta*. I. Kinematics of hovering and forward flight. *J. Exp. Biol.* **200**, 2705–2722.

Willmott, A. P., Ellington, C. P. & Thomas, A. L. R. 1997 Flow visualization and unsteady aerodynamics in the flight of the hawkmoth, *Manduca sexta*. *Phil. Trans. R. Soc. B* **352**, 303–316.

Wunderlich, W. 1978 Approximate optimization of Watt's straight-line mechanism. *Mech. Mach. Theory* **13**, 155–160.

Żbikowski, R. 1999*a* Flapping wing autonomous micro air vehicles: research programme outline. In *Fourteenth International Conference on Unmanned Air Vehicle Systems*. Supplementary Papers, pp. 38.1–38.5.

Żbikowski, R. 1999*b* Flapping wing micro air vehicle: a guided platform for microsensors. In *Royal Aeronautical Society Conference on Nanotechnology and Microengineering for Future Guided Weapons*, pp. 1.1–1.11.

Żbikowski, R. 2000 Flapping wing technology. In *European Military Rotorcraft Symposium, Shrivenham, UK, 21–23 March 2000*, pp. 1–7.

Żbikowski, R. 2002*a* Aerodynamics: red admiral agility. *Nature* **420**, 615–618.

Żbikowski, R. 2002*b* On aerodynamic modelling of an insect-like flapping wing in hover for micro air vehicles. *Phil. Trans. R. Soc. A* **360**, 273–290.

Żbikowski, R., Galiński, C. & Pedersen, C. B. In press. A four-bar linkage mechanism for insect-like flapping wings in hover: concept and an outline of its realisation. *J. Mech. Des.*